Cosmic Ray Muon Simulation to the MINOS Near Detector Depth

Susan Kasahara

March 5, 2007

Abstract

This paper describes a full three-dimensional simulation of cosmic ray muons to the MINOS near detector depth. The paper describes the details of the simulation. A future companion paper will discuss results of the simulation and compare them to expectations.

1 Introduction

Beyond forming a background for neutrino events in the near detector, cosmic ray muons are of use in the calibration of the detector as well as having physics interest of their own. Of particular interest for calibration purposes is the energy distribution of the muons at the near detector site, which differs significantly from that at the far detector site. Of particular interest for physics purposes is the charge ratio of the muons[1], since the shielding afforded by the ~ 100 m of rock overburden above the detector corresponds to a surface threshold energy of ~ 60 GeV for the cosmic ray muons to penetrate to the near detector depth, an energy region above which the MINOS near detector measurement of charge ratio should be competitive with other experimental data.(See reference [2] for a compilation.) A full simulation can be used to determine the expected rate, energy distribution and multiplicity of the events, as well as other attributes that can be useful in the analysis of the data.

The simulation described in this paper is also described on a web site[3] and the simulated data to the near detector depth is available for download on that site. The simulated muons at the near detector depth have been propagated through the near detector geometry by Pat Ward using GMINOS, and are available for download in "reroot" format at a Cambridge Monte Carlo web site[4].

2 Simulation Description

The simulation of cosmic rays to the near detector depth consists of a parameterization of the input cosmic ray primaries at the top of the atmosphere, a

simulation of the atmospheric cascade resulting in the production of high energy muons at the earth's surface, and a simulation of the propagation of the muons through the rock overburden.

This process of simulating the cosmic ray muon background to the MINOS near detector depth is very similar to that in my thesis[5][6] work involving the simulation of cosmic ray muons to the Soudan 2 detector depth. The principle differences between the Soudan 2 simulation and this simulation being:

- The energy threshold imposed by the rock overburden at the near detector ($\sim$ 60 GeV) is much lower than that at the Soudan 2 detector($\sim$ 700 GeV), and this required introducing low energy extensions to both the cascade simulation and cosmic ray primary model.
- Site specific conditions, specifically:
  - The near detector local geomagnetic field.
  - The near detector rock overburden.

  The site specific conditions were researched and implemented as described below.

The description of the simulation in this note will focus on the differences between this simulation and the Soudan 2 simulation.

2.1 Primary Composition Model

The primary cosmic rays are modeled with a parameterized form dependent on the primary energy and type. The parameterized model of the primary spectra used in this case is that of the New Source_P model[6] used in the Soudan 2 simulation, except that the model was extended to lower energies as required by the lower energy threshold ($\sim$60 GeV) imposed by the shallower rock overburden at the near detector site.

The input primary model has the following characteristics:

- The primary cosmic rays are treated as five mass groups centered around the nuclei H,He,CNO,Ne-S, and Fe.
- The model fits the available (circa 1997) satellite and balloon direct measurement data in the low energy region ($<$ 1000 TeV/nucleus) for which this data is available.
- The model is normalized to the air-shower determined all-particle spectrum at higher energies beyond the direct measurement data.

The primary model used in this simulation is shown in Figure 1 along with the direct measurement data to which it was normalized. Figure 2 shows the all-particle spectrum that this model yields and a comparison to air shower data in the "knee" energy region and above.

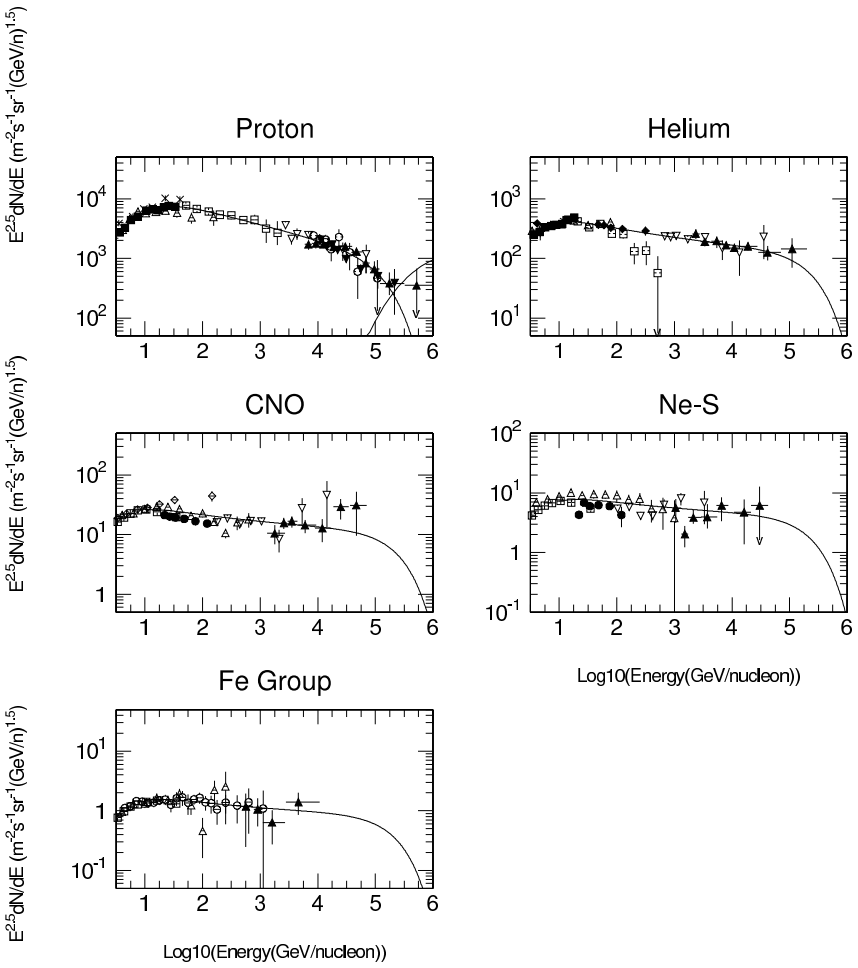

Figure 1: The parameterized form of the primary composition model overlaying the direct measurement data to which it was normalized. This is the same as Figure 5 in reference[6], but the "modulation" factor, $(1+\alpha \mathrm{E}^{-\beta})^{-1}$ at low energy which was neglected in that simulation has been included in this simulation. The references to the direct measurement data can be found in reference[6].

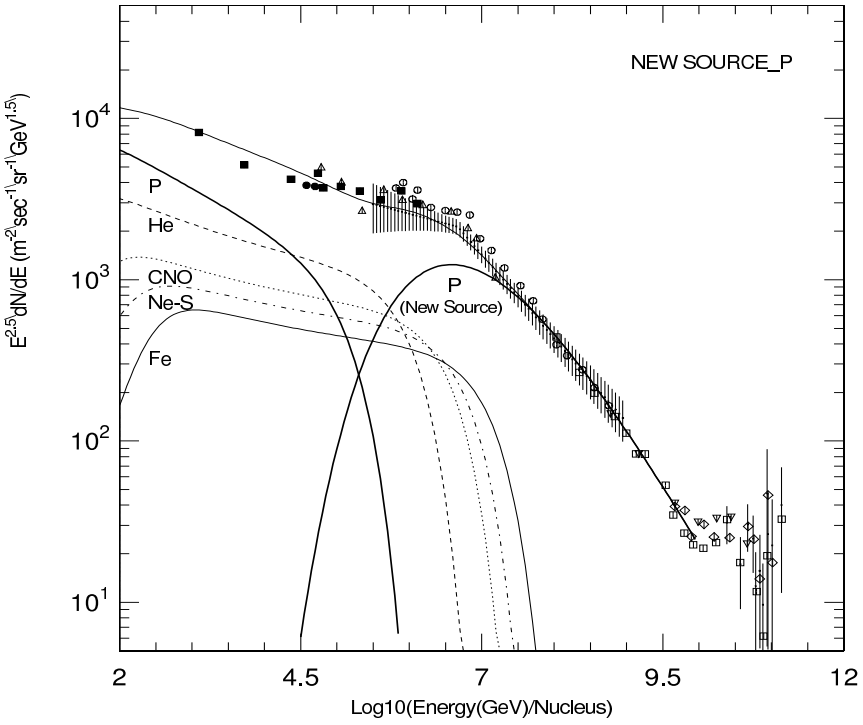

Figure 2: The primary composition model used in this analysis as compared to the all-particle spectrum. The references to the all-particle data can be found in reference[6].

Mass Group	Zeff	Aeff	K1	K2	α	β	E_{cut}
H	1	1	20830	0	1.5	34	1.5E5
He	2	4	7750	840	1.9	201	1.0E6
CNO	7	14	3545	550	1.8	1160	3.5E6
Ne-S	12	24	2655	445	1.5	1180	6.0E6
Fe	26	56	2120	335	1.7	13300	1.3E7

Table 1: Low energy parameters of the New Source_P primary composition model. These are the same parameters as was used in reference[6], with the addition of the new modulation parameters α and β.The unit of K1 and K2 is $(\mathrm{m}^{-2}\mathrm{s}^{-1}\mathrm{sr}^{-1}(\mathrm{GeV/nucleus})^{\gamma 1,2-1})$. The unit of β and E_{cut} is $(\mathrm{GeV/nucleus})^{-1}$.

The New Source_P model consists of a low energy component with a parameterized form:

$$\frac{dN}{dE} = \frac{(K_1 E^{-2.75} + K_2 E^{-2.5}) e^{-E/E_{cut}}}{1 + \alpha E^{-\beta}} \tag{1}$$

applicable to each of the 5 mass groups. The parameters for each of the 5 mass groups are given in Table 2.1.

It also consists of a high energy "New Source" proton component, which has the form given in reference[6] and shown in Figure 2. This high energy component will have little affect on the simulated muon flux, since most near detector muons will be produced by primaries with energies well below the energies at which it becomes significant.

The parameterized form for the differential flux of each component of the model is not integrable, so the procedure for using the model in this simulation required numerical integration to produce a probability table for each component, from which the energy and component type are selected at run time.

2.2 Atmospheric Simulation

The atmospheric cascade simulation is a full 3-dimensional cascade simulation resulting in the production and transport of muons to the surface of the earth. The simulation used here is the HEMAS[7] simulation used in the Soudan 2 simulation[6][5], but adapted for use at the near detector. These adaptations were:

- The cascade simulation was modified to include muon ionization loss in the atmosphere. A neglible effect for the high energy muons relevant to the Soudan 2 detector site, muon ionization loss has a noticable effect on low energy muons in the 10's of GeV energy range or below.
- The appropriate parameters for the local geomagnetic field were included (see below).

- A low energy hadronic interaction model, TARGET[8] was introduced to supplement the high energy hadronic interaction model, SIBYLL [9]. The TARGET model[8] was used in the energy region $E_{lab} < 200$ GeV.

Because the cascade simulation uses a model for the atmosphere which is flat, ignoring the earth's curvature, the simulation was limited to zenith angles in the region $0-70^o$ for which the flat atmosphere/earth approximation is valid. All azimuthal angles are included in the simulation.

The cascade simulation generates particles to the observation level of 228 meters above sea level, the elevation of the surface above the near detector[10]. At the surface, muons were stored for simulation through the separate simulation of the rock overburden as described below.

2.2.1 Local Geomagnetic Field

The geomagnetic field at the MINOS near detector site is near vertical with a strength of 0.56 Gauss and a magnetic inclination and declination of 70.42 degrees and 1.98 degrees W respectively. A diagram of the local field is shown in Figure 3

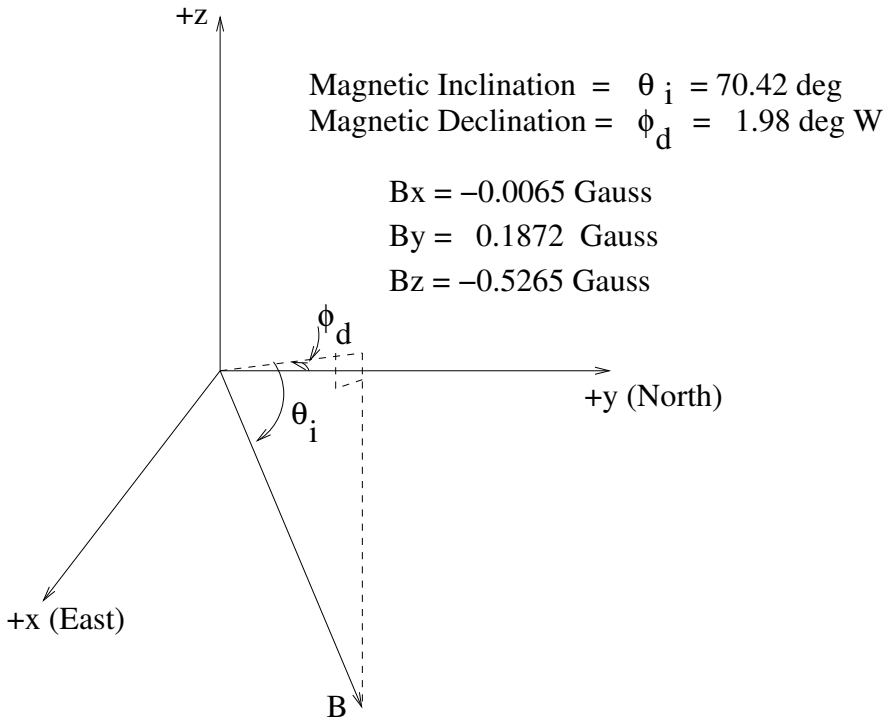

Figure 3: Local geomagnetic field at the near detector site.

The local geomagnetic field was found using the National GeoPhysical Data

Center program GEOMAG[11], using the local coordinates of the near detector[12]:

Lon :	88°	16′	14.2351″	W
Lat :	41°	50′	26.0280″	N

and the near detector surface elevation of 228 m.s.l.

The geomagnetic field was treated as locally uniform in the simulation, a good approximation given that the flight path of secondaries through the atmosphere (< 100 km) is small compared to the radius of the earth.

2.3 Validation of Primary Model and Atmospheric Simulation

The input primary model and atmospheric cascade simulation were tested by comparing the results of the simulation against surface muon experimental data at sea level. The comparison was done at two different zenith angles, 0 and 75 degrees, for which such data is available.

This comparison is shown in Figure 4 for zenith angle 0 degrees, and Figure 5 for zenith angle 75 degrees. The simulation results are in good agreement with the data at both zenith angles, down to the lowest surface muon momentum considered in the simulation which was 40 GeV/c.

Of interest is how well a commonly used parameterization for the surface cosmic ray muon flux[17]:

$$\frac{dN_\mu}{dE} = 0.14 E_\mu^{-2.7} \Big(\frac{1}{1 + \frac{1.1 E_\mu cos\theta}{115 GeV}} + \frac{0.054}{1 + \frac{1.1 E_\mu cos\theta}{850 GeV}} \Big) \quad \mathrm{cm}^{-2}\mathrm{s}^{-1}\mathrm{sr}^{-1}\mathrm{GeV}^{-1} \quad (2)$$

fits the distributions shown in Figure 4 and Figure 5. Equation 2 is shown in the figures to be in good agreement with the data and Monte Carlo simulation at zenith angle 0 degrees, but it agrees less well at zenith angle 75 degrees.

2.4 Simulation through Rock Overburden

The propagation of muons through the rock was simulated using GEANT[18]. GEANT was chosen in place of a simple parameterized form for energy loss because it properly simulates the energy loss mechanisms appropriate for high energy muons, the fluctuations in energy loss and multiple scattering.

An analysis of muon propagation through the rock from the surface to the MINOS near detector level requires knowledge of the rock overburden. The rock overburden at the near detector site as used in this simulation is shown in Figure 6, and consisted of two layers: Glacial Till and Dolomite/Shale Bedrock. The thickness, composition and density of each layer are as shown in the figure and they were determined as is described in the following sections.

2.4.1 Elevation

The surface topography in the region of the near detector is relatively flat. Reference[10] reports elevations varying from 226 to 228 msl in the "project

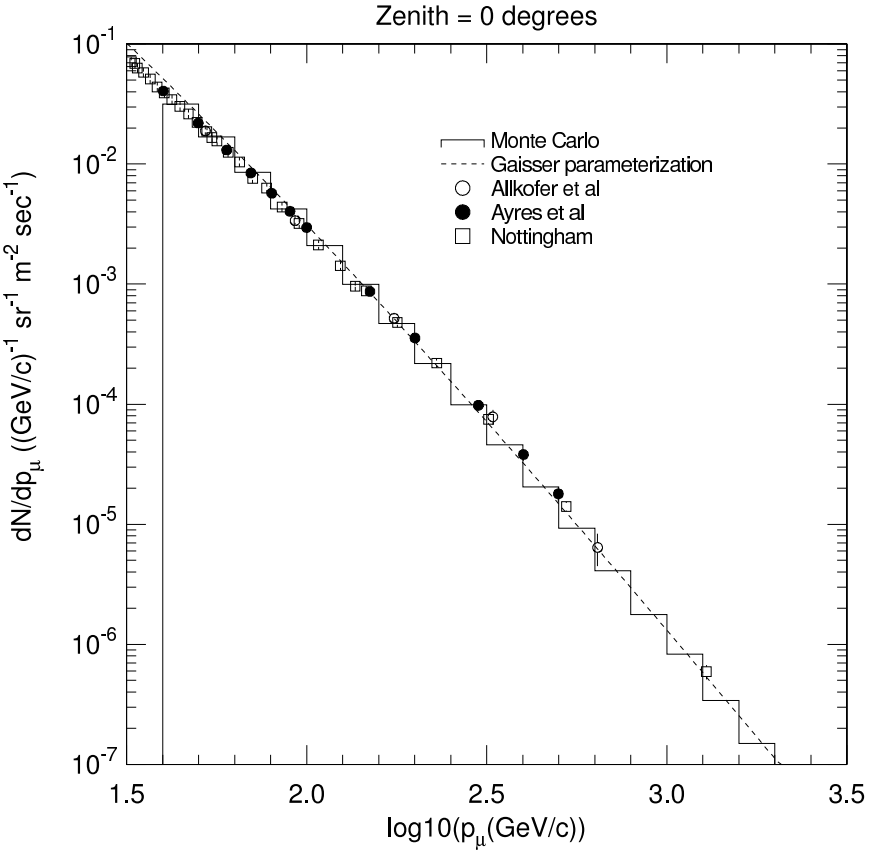

Figure 4: Surface muon rates at sea level for zenith angle 0 degrees. The Monte Carlo simulation results are generated as described in the text. The experimental data results are from references[13, 14, 15]

.

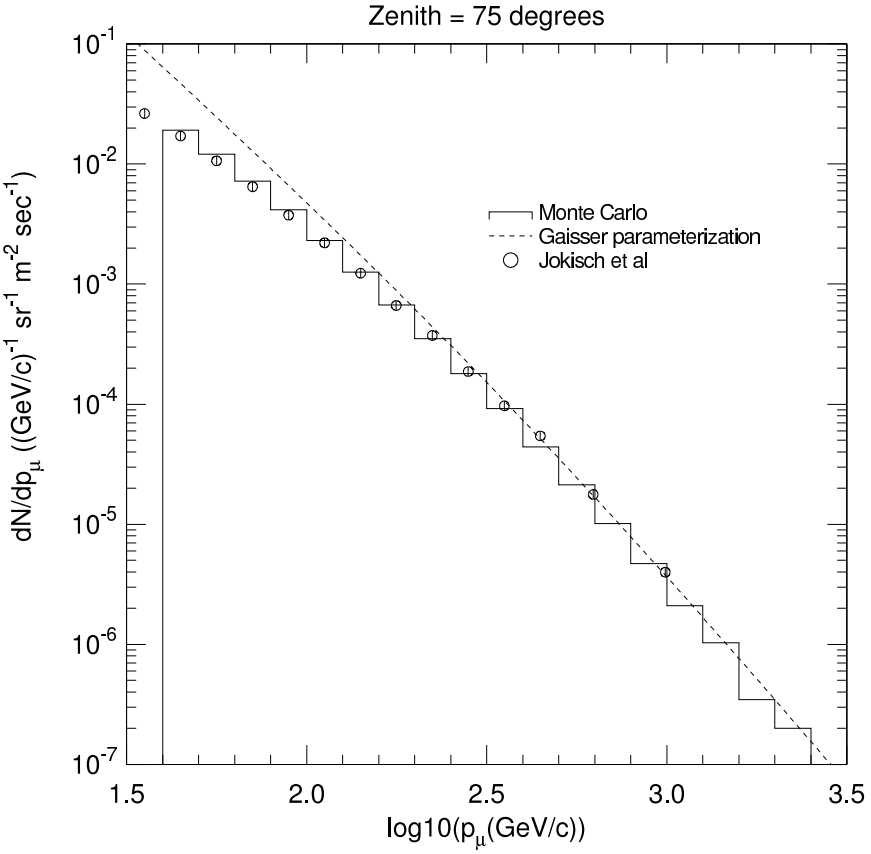

Figure 5: Surface muon rates at sea level for zenith angle 75 degrees. The Monte Carlo simulation results are generated as described in the tex. The experimental data results are from references[16]

.

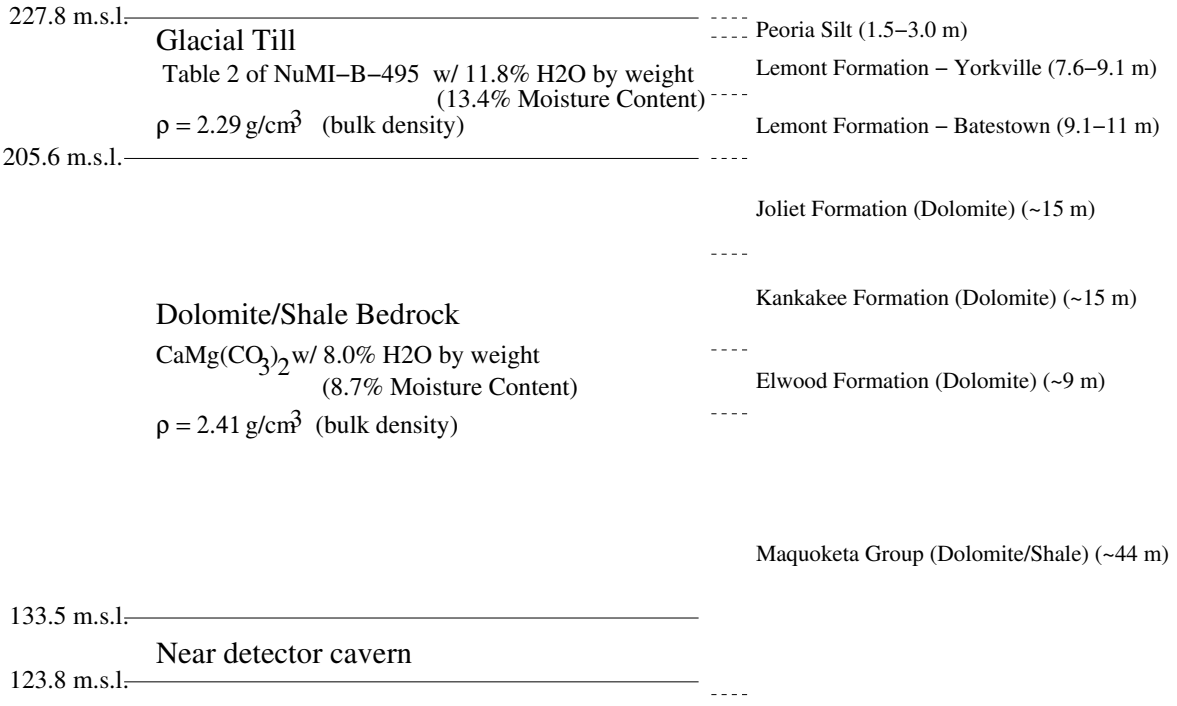

Figure 6: Rock overburden at the near detector site. The values shown here were determined as described in the text.

Formation	Matrix Density (g/cm^3)	Bulk Density (g/cm^3)	Bedrock Porosity (%)
Silurian Dolomite	2.78	2.44	≈ 19
Upper portion (Dolomitic) of Scales formation (Maquoketa)	2.65	2.37	16.6
Lower portion (Shalely) of Scales formation (Maquoketa)	2.84	2.43	≈ 22

Table 2: Average matrix density, bulk density, and bedrock porosity values reported in Table 4 of reference[20] for three layers of near detector bedrock. Silurian Dolomite is characteristic of the upper bedrock according to Table 3 of the same reference. The Scales formation (Maquoketa) is representative of the lower bedrock.

area range" which includes the approximately three quarters mile long region from the Main Injector to the near detector cavern site. For the purposes of this simulation, the surface elevation was taken to be flat.

The elevation above sea level of the surface and Glacial Till/Bedrock boundary were taken from Exhibit 8 of reference[10], reproduced as Figure 7 here. Figure 7 shows the layering of rock in the overburden above and around the near detector cavern. The figure also shows three boring sample tunnels, labeled with names prefaced with "S". (Additional boring samples were taken in regions not included in this figure, but discussed in reference[10].) The boring sample S1247 passes through the near detector cavern, and the surface elevation and Glacial Till/Bedrock boundary were taken to be those as determined from this sample. These values are 227.8 m.s.l. for the surface elevation, and 205.6 m.s.l. for the Glacial Till/Bedrock boundary.

The elevation of the cavern ceiling and floor, 133.5 and 123.8 m.s.l., are from reference[19].

2.4.2 Bedrock

The density and moisture content of the bedrock was determined from the description in Appendix C of reference[20] and the data in Table 4 of that same reference. Four columns of data from Table 4 in that reference are reproduced in Table 2.4.2 for convenience. The values in the table were determined from averages of laboratory measurements on boring samples from several different depths in the range 29 m to 100 m below the surface.

The rock "matrix density", ρ_r, is defined as the density of dry rock. The average rock matrix density of the values reported in Table 2.4.2 is $\rho_r = 2.76$ g/cm^3.

The "bulk density" is defined as the amount of mass in a unit volume of bedrock formation, including water content. The bulk density of bedrock used in this simulation was taken to be the average of the bulk density values reported

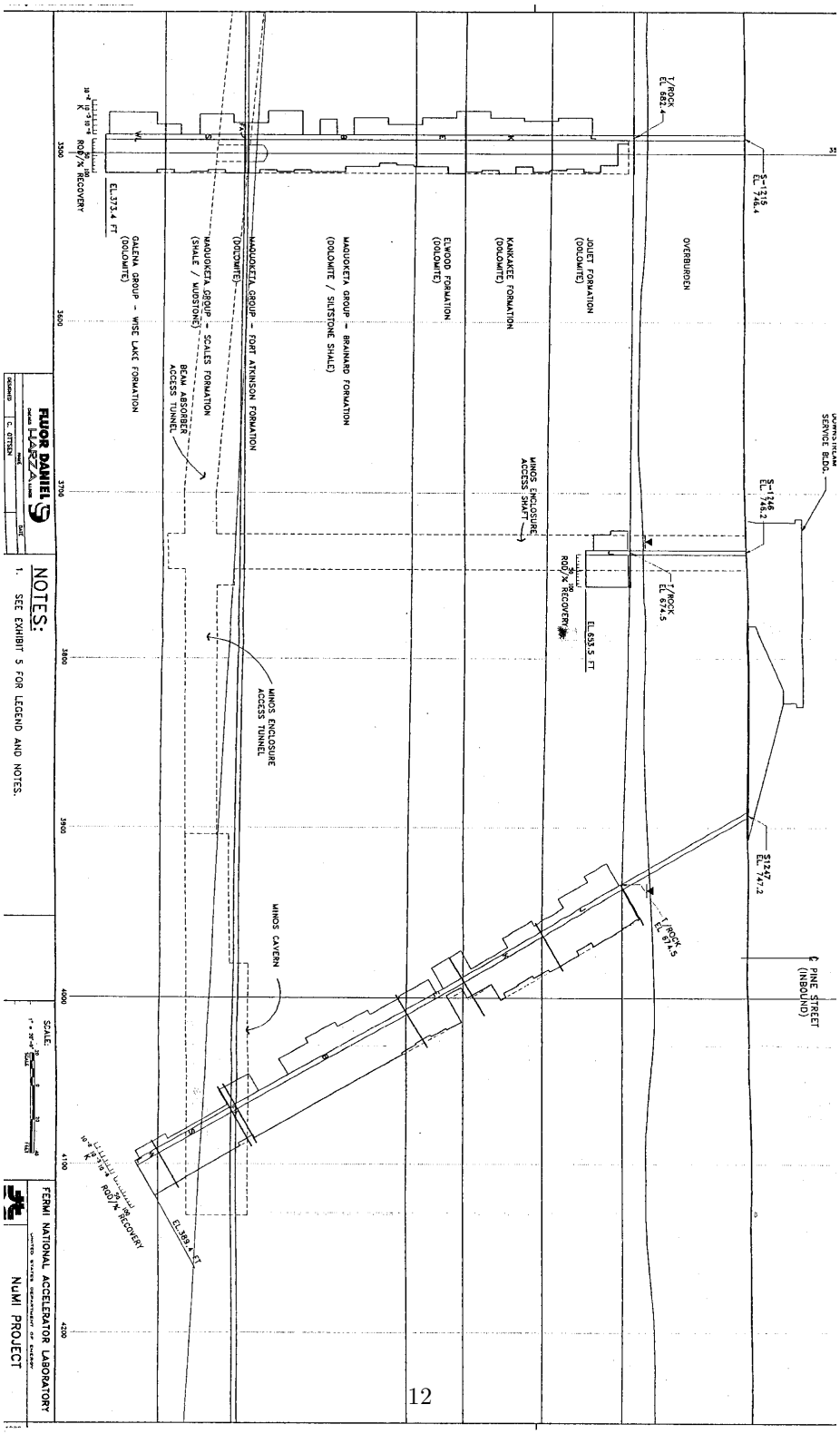

Figure 7: Exhibit 8 of reference[10]. The near detector cavern is in the lower right quadrant.

in Table 2.4.2, or $\rho_{bulk} = 2.41$ g/cm^3.

The bedrock is porous, with the porosity, n, defined to be:

$$n = \frac{V_w}{V_w + V_r} \tag{3}$$

where V_w is the void space in the boring sample, presumed to be filled with water when in situ, and V_r is the volume occupied by rock. The average bedrock porosity was taken to be the average of the porosity values reported in Table 2.4.2, or n=19.2%.

The moisture content by weight is then

$$\begin{aligned} \text{moisture by weight} &= \frac{V_w \cdot \rho_w}{V_w \cdot \rho_w + V_r \cdot \rho_r} && (4) \\ &= \frac{n \cdot \rho_w}{\rho_{bulk}} && (5) \end{aligned}$$

yielding a moisture content by weight for bedrock of 8.0%. "Moisture content", u, is the amount of water in the bedrock, expressed as a percentage of the rock dry weight. This is

$$\begin{aligned} u &= \frac{V_w \cdot \rho_w}{V_r \cdot \rho_r} && (6) \\ &= \frac{n \cdot \rho_w}{\rho_{bulk} - n \cdot \rho_w} && (7) \end{aligned}$$

yielding a moisture content for bedrock of 8.7%.

The composition of the bedrock used in the simulation, $CaMg(CO_3)_2$, is textbook Dolomite mineral.

2.4.3 Glacial Till

Similarly, the bulk density and moisture content of the glacial till was determined from data samples as reported in Table 1 and 2 of reference [10]. The moisture content was taken as the average of values given in the two tables and yields u = 13.4%. The bulk density was calculated from this and the "Dry Unit Weight", ρ_{dry}, as reported in these tables, which is actually a density determined as the mass of the rock sample dry, m_r, over the total volume of the sample:

$$\rho_{dry} = \frac{m_r}{V_r + V_w} \tag{8}$$

In terms of ρ_{dry} and the moisture content, u, the bulk density was obtained for each of the two samples using:

$$\rho_{bulk} = \rho_{dry} \cdot (1 + u) \tag{9}$$

and the average of the two was taken to yield the value $\rho_{bulk} = 2.29$ g/cm^3 as shown in Figure 6.

Element	Z	A	Weight Fraction
Silicon	14	28	0.1447
Aluminum	13	27	0.0244
Iron	26	56	0.011
Calcium	20	40	0.07
Magnesium	12	25	0.0379
Carbon	6	12	0.0512
Sodium	11	23	0.0034
Potassium	19	39	0.00814
Oxygen	8	16	0.64

Table 3: Composition of glacial till from Table 2 of reference[21], which references[22].

The moisture content by weight of the glacial till is determined using Equation 5 and the above values for n and ρ_{bulk} to be 11.8%.

The composition of the glacial till is taken from that of Table 2 of reference [21] which in turn references [22]. This composition is shown in Table 2.4.3 and is that used in the simulation.

2.4.4 Transmission Probability

The GEANT simulation implemented with the rock overburden shown in Figure 6 was used to determine the transmission probability for a muon at the surface to reach the underground near detector depth as a function of muon surface energy. The transmission probability plot for muons with zenith angle zero degrees is shown in Figure 8. This plot shows that vertical muons with a surface energy of ~ 55 GeV will reach the near detector depth approximately 50% of the time. The plot is not a step function because of energy loss fluctuations, which become increasingly important at higher zenith angles due to the higher muon energies required to penetrate greater slant depths.

3 Conclusion

A full three-dimensional simulation of cosmic ray muons to the MINOS near detector depth has been described. The results of this simulation will be compared to expectations in a future companion paper.

References

[1] J. de Jong. A first look at a charge ratio measurement at the near detector. NuMI 2549, Fermi National Accelerator Laboratory, 2006.

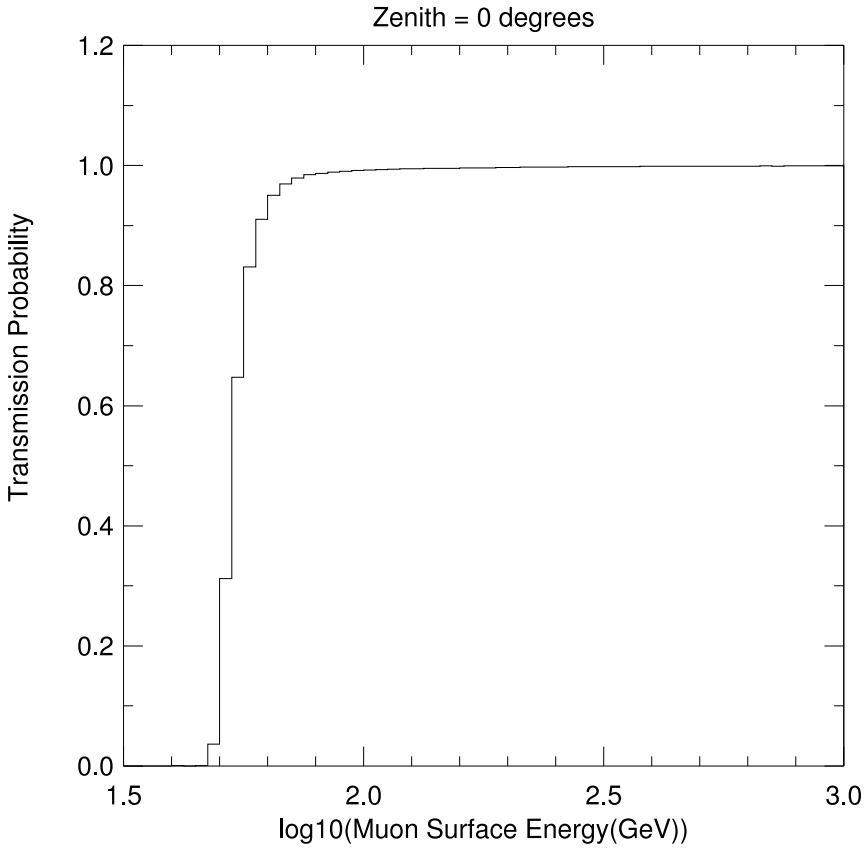

Figure 8: The transmission probability of a surface muon as a function of the surface muon energy for zenith angle 0 degrees.

.

[2] T. Hebbeker and C. Timmermans. A compilation of high energy atmospheric muon data at sea level. *Astropart. Phys.*, 18:107, 2002.

[3] S. Kasahara. http://www.hep.umn.edu/∼schubert/near/.

[4] P. Ward. http://www.hep.phy.cam.ac.uk/minos/group/mc/mc.html.

[5] S.M. Kasahara. *A study of cosmic ray composition in the knee region using multiple muon events in the Soudan 2 detector*. PhD thesis, University of Minnesota, 1997.

[6] S.M. Kasahara *et al.* A study of cosmic ray composition in the knee region using multiple muon events in the Soudan 2 detector. *Phys. Rev. D*, 55:5282, 1997.

[7] C. Forti *et al.* Simulation of atmospheric cascades and deep-underground muons. *Phys. Rev. D*, 42:3668, 1990.

[8] T.K. Gaisser *et al.* Nuclear target effects and interpretation of cosmic ray cascades. *Proc. 18th Int. Cosmic Ray Conf. (Bangalore)*, 5:174, 1983.

[9] R.S. Fletcher *et al.* Sibyll: An event generator for simulation of high energy cosmic ray cascades. *Phys. Rev. D*, 50:5710, 1994.

[10] Inc. Fluor Daniel and Harza Engineering Co. NuMI project geotechnical data report. Technical report, 1998.

[11] National Geophysical Data Center. http://www.ngdc.noaa.gov/seg/geomag/. Note that the geomagnetic field changes slowly with time and the values obtained depend on the input date.

[12] W. Smart. Private communication, April 7, 2003.

[13] O.C. Allkofer *et al.* The absolute cosmic ray muon spectrum at sea level. *Phys. Letters B*, 36:425, 1971.

[14] C.A. Ayre *et al.* Precise measurement of the vertical muon spectrum in the range 20-500 GeV/c. *Journal of Physics G*, 1:584, 1975.

[15] B.C. Rastin. A study of the muon charge ratio at sea level within the momentum range 4 to 2000 GeV/c. *J. of Phys. G*, 10:1629, 1984.

[16] H. Jokisch *et al.* Cosmic-ray muon spectrum up to 1 TeV at 75^o zenith angle. *Phys. Rev. D*, 19:1368, 1979.

[17] W.M. *et al* Yao. Review of particle physics. *Journal of Physics G*, 33:1, 2006.

[18] CERN. Geant version 3.21. Technical report.

[19] J.K. Nelson. Private communication, 1999.

[20] A. Wehmann. Concentration levels of inflow in numi sump water. NuMI-B 494, Fermi National Accelerator Laboratory, 1999.

[21] A. Wehmann and S. Childress. Tritium production in the Dolomitic rock adjacent to NuMI beam tunnels. NuMI-B 495, Fermi National Accelerator Laboratory, 1999.

[22] T.B. Borak *et al.* The underground migration of radionuclides produced in soil near high energy proton accelerators. *Health Phys.*, 23:679, 1972.